La mer 45 : 91-98, 2007
Société franco-japonaise d'océanographie, Tokyo

Numerical Radiative Transfer Simulations to Examine Influence of Shape of Scattering Phase Function of Suspended Particles on the Ocean Colour Reflectance

Takafumi HIRATA*,# and Gerald F. MOORE*,#

Abstract: Effects of shape of particle scattering phase function on the ocean colour reflectance are examined by means of radiative transfer simulations. The simulations suggest that different shape of particle phase function may cause 19% of discrepancy in the reflectance for oceanic waters, even if the backscattering probability of suspended particles does not change. The discrepancy can be even larger for absorbing waters in coastal zone.

Keywords: *Ocean Colour Reflectance, Phase Function Effects, Numerical Simulations*

1. Introduction

Numerical simulation of radiative transfer is a useful method to understand and predict variability of the ocean color reflectance from which biogeochemical properties of seawater may be exploited. When opticaliy shallow waters and inelastic scattering (including Raman scattering and fluorescence) are not considered, the time-independent simulations for 1D space (depth) are equivalent to solving the Equation of Radiative Transfer (ERT):

$$\left[\cos\theta\frac{d}{d\tau}+1\right]L(\Omega,\tau)=\omega\int 4\pi L(\Omega'\tau)P(\Psi,\tau)d\Omega' \quad (1)$$

where L and $d\Omega$'represent the radiance and infinitesimal solid angle, respectively. ω is the single scattering albedo and $P(\Psi,\tau)$ is the scattering phase function of seawater. If ω and P are given, the ERT can be solved with respect to L, provided initial and boundary conditions are given. From the solution of the ERT, the ocean colour reflectance can be obtained by R_{rs}= $L_u / \int_0^{2\pi} L\cos\theta_v\, d\Omega' = L_u / Ed$" where θ_v, L_u and E_d are the viewing zenith angle, the upward radiance (i.e. L (θ_v<90°) and the downward irradiance, respectively. Due to difficulties in measuring P, the classic measurements of P taken by PETZOLD (1972) have been assumed in the radiative transfer simulations for analysis of R_{rs}. Effects of this assumption should be evaluated prior to drawing final conclusions.

Only a few evaluations of the assumption exist. PLASS *et al.* (1985) showed that shape of phase function can significantly affect L_u. More recently however, MOBLEY *et al.* (2002) concluded that the exact shape of the phase function in backscattering directions is not critical if the backscattering probability is correct and a 10% of error is acceptable. Thus, results from the two groups do not agree well with each other, and re-examination is required. The objective of this paper is to re-evaluate the influence of the shape of P on R_{rs} by means of numerical simulations and to see whether the use of the single shape of P (i.e. PETZOLD P) is valid for different water types.

2. Simulations

The numerical radiative transfer simulations are made by Hydrolight (MOBLEY, 1995) for R_{rs}

*Centre for observation of Air-Sea Interactions and fluxes (CASIX)
#Plymouth Marine Laboratory, Prospect Place, The Hoe, Plymouth, Devon, PL1 3DH, UK
Corresponding author's Email: tahi@pml.ac.uk

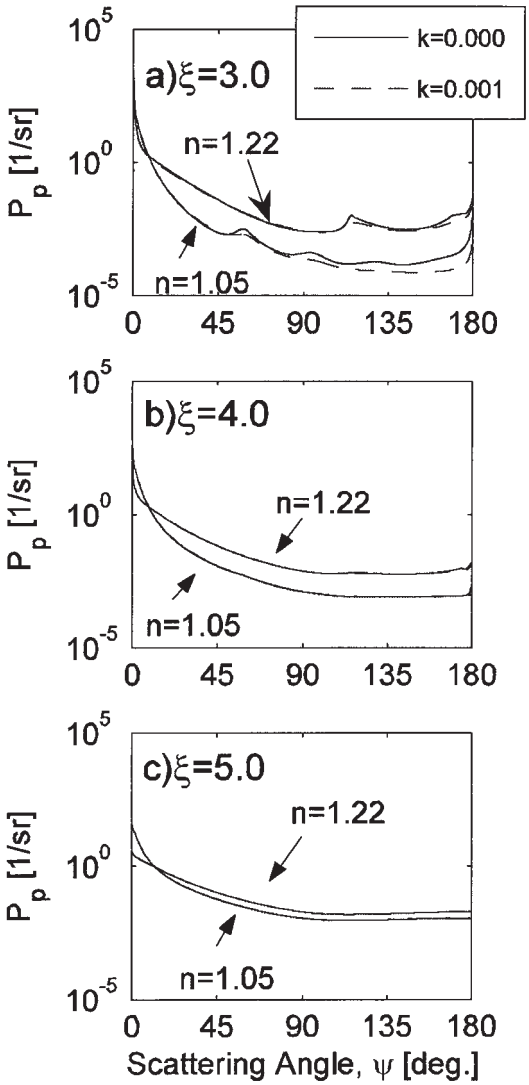

Fig. 1 Phase functions by Lorentz-Mie theory: (a) ξ =3.0 (b) ξ =4.0 and (c) ξ =5.0. Real and imaginary parts of the refractive index are represented by n and k, respectively.

using different shapes of P. The simulated R_{rs} is then compared. In the following, the justification for the phase functions used for the comparison is described.

2.1. Phase function, P

The phase function of seawater P is expressed by a weighted sum of that of pure seawater P_w and suspended particles P_p:

$$P = (1 - W)\, P_w + W P_p. \quad (2)$$

The weighting function W ($\equiv b_p/(b_w+b_p)$) explains a contribution of the particle scattering to the total scattering. Variations in P are caused by variations of P_w, P_p and W. Since variations in P_w are relatively much less than these in P_p and W, variations in P are determined by these in P_p and W in practice.

Due to the lack of sufficient measurements of P_p, Lorentz-Mie computations were performed just to obtain an idea of variability in P_p. In the Lorentz-Mie computations, particle size distribution $N(D)$ was varied according to Junge distribution $N(D) \sim D^{-\xi}$ where N and D represent number of particles and sphere-equivalent diameter of particles, respectively. Junge slope ξ was varied from 3.0 to 5.0. The complex refractive index (n) was varied from 1.05 to 1.22 for the real part to consider algal particles and mineral particles, and 0.0 to 0.001 for the imaginary part (k) to consider absorbing particles. The computations show that the shape of P_p is remarkably variable at small and large angles (Fig. 1). According to GORDON (1993) however, the scattering at the small scattering angles has little effect on the light field. Hence we focus on P_p at large angles, or backscattering angles. The P_p at backscattering angles predicted by Lorentz-Mie theory may be classified into three classes: (I) P_p with a peak at around 180° of scattering angle (Fig. 1a), (II) P_p with no such peak (Fig. 1c) and (III) the intermediate case (Fig. 1b). In order to examine possible maximum effects of phase function on the ocean colour reflectance, two boundary shapes of P_p (i.e. backward-peaked and non-backward-peaked phase functions) are considered.

2.2.1 Backward-peaked phase function of suspended particles

The backward-peaked P_p obtained from Lorenz-Mie computations (Fig. 1a) has a similar shape to that of PETZOLD phase function (shown as a bold curve in Fig. 2) which has a remarkable peak at backward direction. Because the aim of this paper is to examine effects of use of the PETZOLD P_p in ocean colour analysis, the PETZOLD P_p is used here as a reference phase function that represents the backward-peaked P_p at the same time.

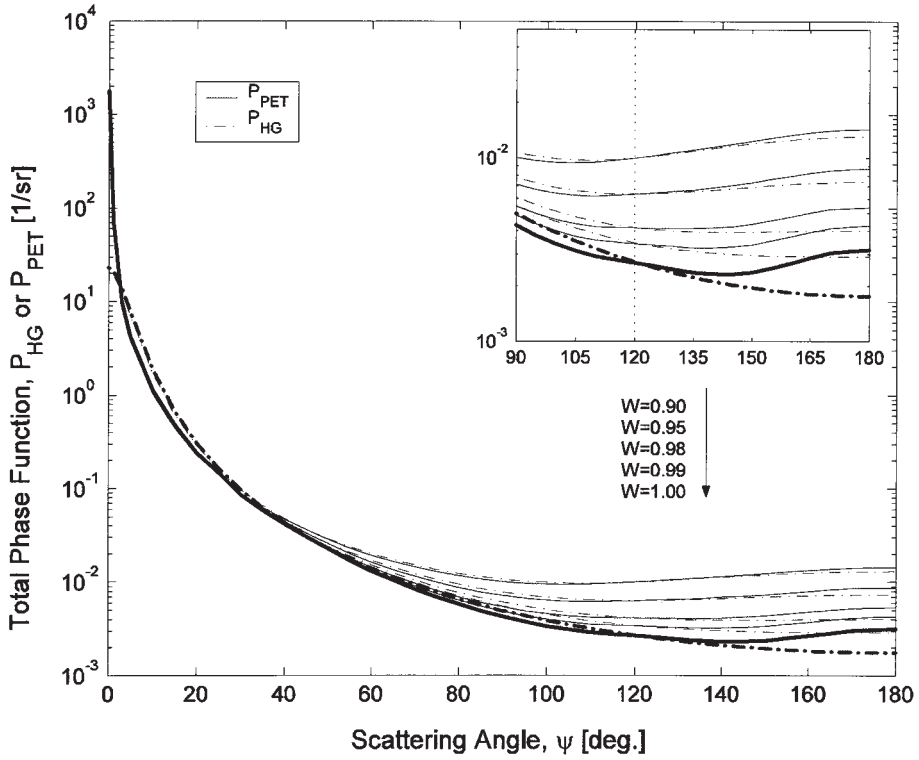

Fig. 2 Total phase function calculated with particle phase function represented by Heyney-Greenstein phase function P_{HG} (dash-dot curves) and PETZOLD phase function P_{PET} (solid curves). From the top to the bottom, W ($=b_b/b_{tot}$) varies from 0.90 to 1.00. Thick curves represent P_{HG} and P_{HG} for W=1.0, or P_{pHG} and P_{pPET} respectively. Subplot is drawn to emphasize the phase functions at the backscattering angle (i.e. $90 \leq \phi \leq 180$).

2.2.2 Non-backward-peaked phase function

The other characteristic shape of P_p predicted from Lorentz-Mie theory has a relatively flat shape in backward scattering angles (i.e. Non-backward-peaked phase function, Fig. 1c). Henyey-Greenstein phase function P_{pHG} represents such a shape:

$$P_{pHG} = \frac{1}{4\pi} \frac{1-g^2}{[1+g^2-2g\mu]^{3/2}} \qquad (3)$$

where g and μ represent the asymmetry factor and cosine of scattering angle. Fig. 2 shows that P_{pHG} (shown as P_{HG} for W=1.0) is similar to the non-backward-peaked P_p predicted by Lorenz-Mie theory shown in Fig. 1c. We use P_{pHG} here to represent the non-backward-peaked P_p, rather than those determined by Lorentz-Mie theory, because P_{pHG} is expressed in an analytical form so that P_p can readily be assigned the same backscattering fraction b_{bp}/b_p as that of PETZOLD P_p. Resultant g used here is 0.9185.

2.2.3 The phase functions of total water

Variations of P calculated with P_{pPET} and P_{pHG} are shown in Fig. 2 for W varying from 0.9 to 1.0. For W=1.0 (bold curves), P is simply either P_{pPET} (solid) or P_{pHG} (dash-dot): see Eq. 2, too. It is seen that shape of backward P calculated from P_{pPET} or P_{pHG} are different only when W exceeds 0.9 due to the large contribution of P_w at W<0.9. P_{HG} has been used to represent P for total (water + particle) seawater, and such approximation is not adequate for oceanic waters (HALTRIN, 2002). However, P_{HG} is used here for an approximation to P_p, not to P. In addition, P_{HG} used as P_p still preserves a physical phenomenon that total P obtained from P_{pHG} has the least variability at the scattering angle of 120 deg. (OISHI, 1990) (see inset of Fig. 2).

Thus, P_{HG} would still be useful for oceanic application as long as it is used as one of the boundary shape of P_p.

2.3. Other input parameters

The radiative transfer simulations require not only P but also the single scattering albedo $\omega = b_{tot} / (a_{tot}+b_{tot})$ as well as initial and boundary conditions. ω is calculated from a_{tot} and b_{tot} which are determined as follows. The absorption coefficient is decomposed into that by pure water (a_w) and by any other substances (a_{py}) so that $a_{tot}=a_w+a_{py}$. Subscript py means particle plus yellow substance. Due to lack of sufficient measurements to define natural variability of a_{py} in the world oceans, a_{py} is numerically varied from 0 to 1.59 m^{-1}; this range of values covers the maximal a_{py} observed in coastal waters by BABIN *et al.* (2003a). Effects of the upper limit chosen will be discussed in Section 3.2. Values of a_w are taken from a measurement made by POPE and FRY (1997). The scattering coefficient may also be decomposed into $b_{tot}=b_w+b_p$ where subscript p means particles. Due to the same reason as a_{py} above, b_p is numerically varied from 0 to 7.37 m^{-1}; such a value of scattering corresponds to a sediment load of 7 to 15 g/m^{-3} (BABIN *et al*, 2003b) and the maximum CHL considered here Selection of the upper limit of b_p will also be discussed in Section 3.2. Values of b_w are taken from MOREL (1974). Table 1 summarizes values of a_{py} and b_p used in the present simulations.

The initial condition to the ERT is determined from HARRISON and COOMBES (1988) and GREGG and CARDER (1990) with variable solar zenith angle (θ_s) from 0 to 75 deg. as shown in Table 1 (Results are shown only up to 58.3 deg. within the geometry for remote sensing, which does not affect a conclusion drawn in this paper). The boundary condition to the ERT is determined from Cox-Munk wave distribution with the wind speed of 7.2 m/s. The ocean is assumed to be optically deep. Actual simulations are performed for 15 discrete optical depths from τ =0 down to τ =7 with 0.5 interval, although we only focus on τ =0 which is relevant remote sensing applications. Wavelength λ is selected based on SeaWiFS bands (Table 1) but restricted to shorter wavelengths to minimise effects of inelastic scattering, including Raman scattering and fluorescence. The simulations are performed for all possible combinations of input parameters above (including any combination between a_{tot} and b_{tot}). Radiance to derive R_{rs} is obtained from 0 to 49° of the viewing zenith angle and from 0 to 180° of the viewing azimuth angles (Table 1).

Table 1 Parameter values used for the simulations. All combinations of the parameters are considered in the simulations. Wavelengths larger than 555 nm are not considered to minimise possible effects of inelastic scattering.

a_{py} [m^{-1}]	b_p [m^{-1}]	Solar zenith angle [deg.]	Viewing zenith angle [deg.]	Viewing azimuth angle [deg.]	Wavelength [nm]
0.000	0.000	0.0	2.0	0	412.5
0.017	0.019	8.3	7.0	15	442.5
0.028	0.038	16.7	13.0	30	490.0
0.046	0.073	25.0	19.0	45	510.0
0.076	0.140	33.0	25.0	60	555.0
0.126	0.271	41.7	31.0	75	
0.209	0.525	50.0	37.0	90	
0.347	1.017	58.3	44.0	105	
0.576	1.967	66.7	49.0	120	
0.956	3.807	75.0	55.0	135	
1.587	7.368		61.0	150	
			67.0	165	
			73.0	180	
			79.0		
			85.0		

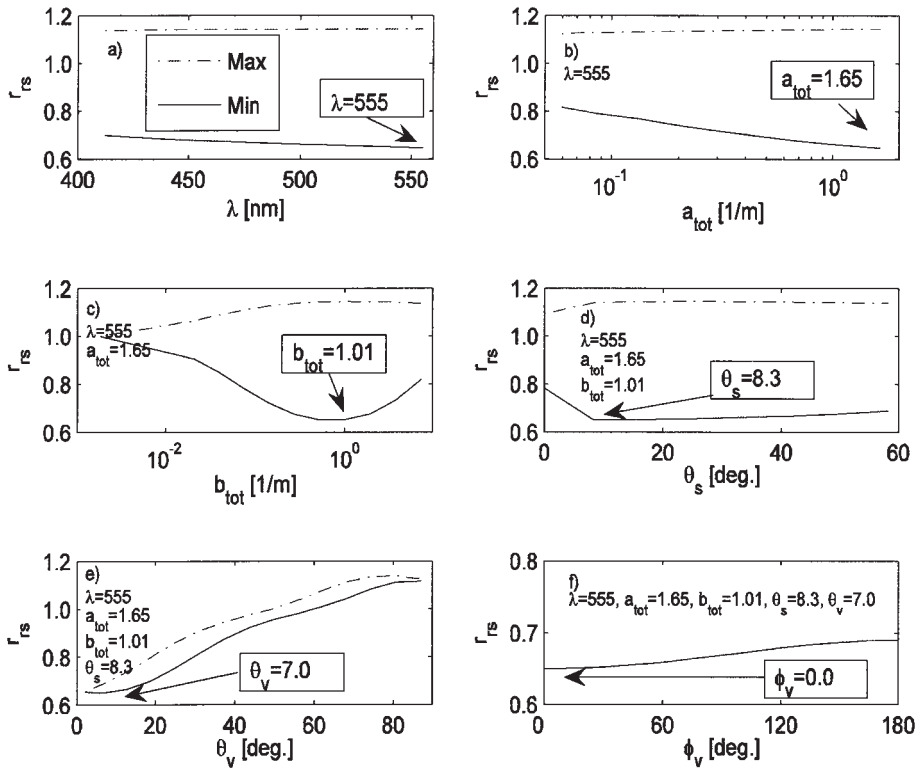

Fig. 3. Maximum and minimum values of r_{rs} ($=R_{rsHG}$ / R_{rsPET}): (a) as a function of only λ. All of range of other parameters is considered; (b) as a function of only a_{tot} but λ is fixed at 555 nm; (c) as a function of b_{tot} at λ =555 nm and at a_{tot} =1.65 m^{-1}; (d) as a function of θ_s at λ =555 nm, a_{tot} =1.65 m^{-1}, and b_{tot} =1.01 m^{-1}; (e) as a function of θ_v at λ =555 nm, a_{tot} =1.65 m^{-1}, b_{tot} =1.01 $m^{-1}$and θ_s=8.30°; (f) as a function of ϕ v at λ =555 nm, a_{tot} =1.65 m^{-1}, b_{tot} =1.01 m^{-1}, θ_s=8.30° and θ_v=7.00°.

3. Results and discussions

The influence of P may be described by the ratio between R_{rs} simulated with P_{pPET} (denoted by R_{rsPET} hereafter) and R_{rs} simulated with P_{pHG} (R_{rsHG}): i.e. $r_{rs} = R_{rsHG}/R_{rsPET}$. The influence of P_p is shown by the deviation of r_{rs} from unity, and the largest influence can be evaluated by either of the maximum or minimum value of r_{rs}.

3.1 Estimation of the largest influence

Fig. 3a depicts r_{rs} as a function of only λ. All other variables, such as inherent optical properties (i.e. a_{tot} and b_{tot}, or ω) and viewing and illumination angles, were varied. The maximum value of r_{rs} ($\approx$1.16) is almost independent of λ. The minimum values of r_{rs} decreases from 0.70 to 0.65 as λ increases. Since deviation of the minimum r_{rs} from unity is larger than deviation of maximum r_{rs} from unity at all λ, the maximum discrepancy between R_{rsHG} and R_{rsPET} is represented by the minimum r_{rs}. The largest influence of P_p is found at λ =555 nm.

Fig. 3b shows r_{rs} as a function of only a_{tot} but wavelength is now fixed at 555 nm. All other variables except λ are allowed to vary. The maximum values of r_{rs} are almost constant while the minimum values of r_{rs} decrease with a_{tot}. Since the greatest deviation of the minimum r_{rs} from unity is larger than that of maximum r_{rs}, the largest influence of P_p is found by the minimum r_{rs} at a_{tot}=1.65 m^{-1}.

Fig. 3c shows r_{rs} as a function of only b_{tot} but now λ and a_{tot} are fixed at 555 nm and 1.65 m^{-1}, respectively. Variation of the minimum r_{rs} is not monotonic. It firstly decreases and then increases, as b_{tot} increases. Since the greatest deviation of the minimum r_{rs} from unity is larger than that of maximum r_{rs}, the largest

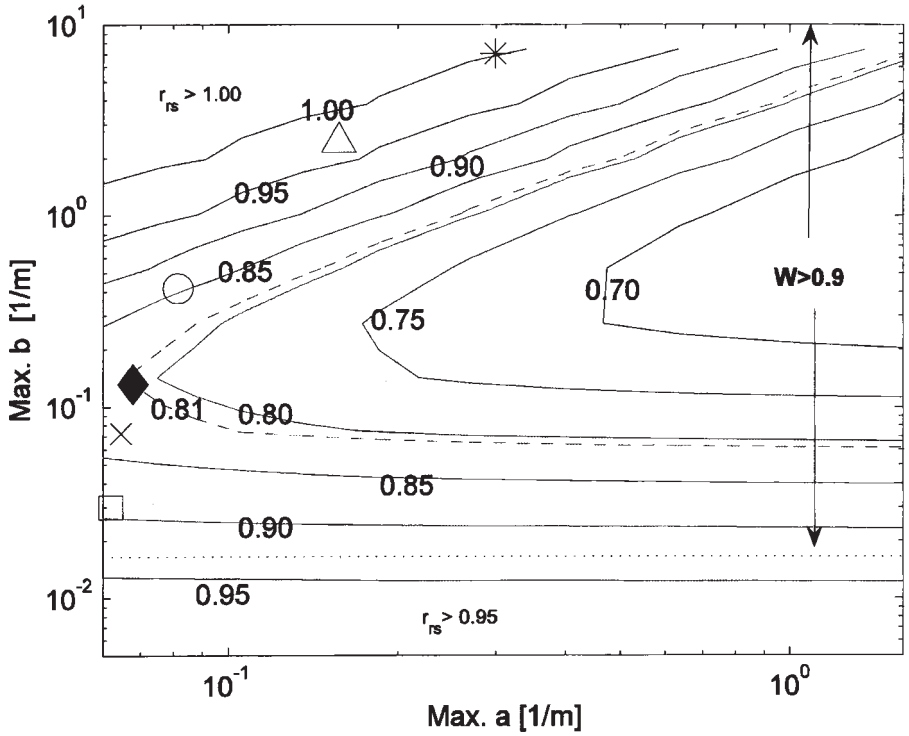

Fig. 4 Contour plot of r_{rs} as a function of upper limits of a_{tot} and b_{tot}. Chlorophyll a concentrations are specified by: □ =0.03, × =0.10, ◆=0.22, o=1.00, Δ=10.0, ＊=40.0mg/m^{-3}. Dotted line shows a boundary for W>0.9. Dashed curve is drawn especially for r_{rs} =0.81.

influence of P_p occurs at b_{tot}= 1.01 m^{-1}.

r_{rs} at λ =555 nm, a_{tot}=1.65 m^{-1} and b_{tot}=1.01 m^{-1} is shown in Fig. 3d as a function of solar zenith angle θ_s. The largest influence of P_p is found when θ_s=8.30 deg. Fig. 3e shows r_{rs} at λ =555 nm, a_{tot}=1.65 m^{-1}, b_{tot}=1.01 m^{-1} and θ_s =8.30 deg. as a function of the viewing zenith angle θ_v, in which the largest influence is found at θ_v=7.00 deg. Finally ϕ_v at which the largest influence of phase function is found is 0 deg, in which case r_{rs}=0.65. (Fig. 3f).

The largest influence of particle phase function is found at λ =555 nm, a_{tot}=1.65 m^{-1}, b_{tot} =1.01 m^{-1}, θ_s=8.30 deg., θ_v=7.00 deg., and ϕ_v= 0 deg. with r_{rs} =0.65, indicating that the influence of P_p can be significant to cause 35%=100 (1−0.65) of maximum discrepancy in R_{rs} according to the present simulations.

3.2 Effects of choice in upper limit of a_{tot} and b_{tot}

In the results shown above, the largest influence of P_p was found at a_{tot}=1.65 m^{-1} which is the upper limit of a_{tot} set in our simulations. Also the largest influence of phase function as a function of b_{tot} did not show a constant effect over b_{tot}. These mean that our results obtained earlier depend on the choise of the upper limit of a_{tot} and b_{tot}, or equivalently a_{py} and b_p since a_w and b_w are regarded as constants. for each waveleugth In order to see effects of this choice, simulations are repeated by changing the upper limit of a_{tot} and b_{tot} (denoted hereafter by Max a_{tot} and Max b_{tot}, respectively). Fig. 4 shows the largest influence of P_p in terms of r_{rs}, as functions of Max a_{tot} and Max b_{tot}. If Max a_{tot} assumed in simulations is larger / smaller than "real" upper limit of a_{tot}, the largest influence of phase function is over/under-estimated when Max b_{tot} is relatively large. When Max b_{tot} is relatively small however, the over/under estimation is less severe or even negligible, even if Max a_{tot} is incorrectly selected. This is consistent with Section 2.2.3 that the phase function

effects are remarkable only when W>0.9.

If Max b_{tot} assumed is relatively larger/smaller than actual upper limit of b_{tot} the largest influence of P_p simulated is over/under-estimated, when the magnitude of actual b_{tot} is small. When the magnitude of actual b_{tot} itself is large however, the largest influence of P_p simulated will be under/over-estimated if Max b_{tot} assumed is relatively larger/smaller than actual upper limit of b_{tot}. The above results indicate that precise determination of the upper limit of a_{tot} and b_{tot} is required for quantitative prediction of the influence of P_p.

MOREL and MARITORENA (2001) proposed statistical relationships between a_{tot} (or b_{tot}) and Chlorophyll a concentration (CHL) for oceanic water based on numerous in situ observations, from which natural Max a_{tot} and Max b_{tot} may be determined in terms of an upper limit of CHL since the statistical relationship is non-linear but monotonic. Their data showed nearly 40 mg m^{-3} of the maximum CHL in oceanic waters: see their Fig.3 in MOREL and MARITORENA (2001). Thus, realistic Max a_{tot} and Max b_{tot} can be calculated for oceanic water by using CHL=40 mg m^{-3}. The largest influence of P_p estimated using Max a_{tot} and Max b_{tot} derived in this way are shown in Fig. 4 as a star symbol. The largest influence of P_p for CHL=0.03, 0.1, 1.0 and 10.0 mgm^{-3} are also superimposed for comparison as well as for CHL=0.22 mg m^{-3} which is a global annual average of CHL derived from SeaWiFS. When CHL is 0.22 mg m^{-3}, r_{rs} is 0.81 showing that 100 (1.00-0.81) =19 % of largest influence of P_p. The influence is relatively less for lower and higher CHL. The present result suggests that the influence of P_p on R_{rs} (or equivalently L_u) can be significant for oceanic waters.

For coastal waters, a significant number of observations for a_{tot} and b_{tot} are required to define their maximum variability. Therefore quantitative prediction of the phase function effects cannot be made for coastal waters at the present stage. However, general tendency of the effects for coastal waters can be found at least qualitatively (Fig. 4). For absorbing waters (e.g. Baltic sea) where Max a_{tot} is much larger than that for oceanic waters, the possible largest influence of P_p on R_{rs} will be larger than that for oceanic waters, unless Max b_{tot} (or b_{tot}) is also much larger than b_{tot} for oceanic waters. For scattering waters (e.g. Black sea) where Max b_{tot} is much larger, the largest influence of P_p on R_{rs} will be reduced unless Max a_{tot} is also much larger.

It is clear that a balance between the absorption and scattering play a significant role in the phase function effects, and the absorbing water or scattering waters may be defined based on ω. However, it should be emphasized that absolute magnitude of b_{tot} (or alternatively b_p) must also be considered together with ω when the phase function effects are estimated, since (1) we saw in Section 2.2.3 that significant difference in P is found only at W >0.9 and (2) a value of ω cannot specify a unique value of W.

Phase function effects for the absorbing waters implies that, even for oceanic waters, the effects can be significant at near-infrared wavelengths where the absorption by pure seawater itself is much larger than that at visible wavelengths. The near-infrared has a particular importance for atmospheric correction scheme of the ocean colour imagery, especially when the waters have a significant reflectance in the NIR; the bright pixel assumption (MOORE *et al*, 1999). Thus, the present work implies that the phase function effects need to be considered in remote sensing application.

5. Conclusion

The largest influence of P_p is estimated to be 19% for oceanic waters. For coastal waters, the influence can even be larger in absorbing waters, whereas it can be smaller in scattering waters. The influence of shape of phase function of suspended particles can be significant, especially when intensity of scattering of particle is large enough compared to that of pure seawater (0.9<W). The present results suggest that the shape of P has to be taken into account in the ocean colour analysis, especially in highly absorbing waters.

Acknowledgements

This work was a part of Project 4 “Biogeochemistry of the Open Ocean” in Science Element 2 “Biogeochemistry of the Upper Ocean”

by Centre for Air-Sea Interactions and fluxes (CASIX): CASIX publication number 43. The authors acknowledge financial support from Natural Environmental Research Council (NERC).

References

BABIN, M., D. STRAMSKI, G. M. FERRARI, H. CLAUSTRE, A. BRICAUD, G. OBOLENSKY and N. HOEPFNNER (2003a): Variations in the light absorption coefficients of phytoplankton, nonalgal particles, and dissolved organic matter in coastal waters around Europe, J. Geophys. Res., **108** (C7), 3211, doi:10.1029/2001JC000882.

BABIN, M., A. MOREL, V. FOURNIER-SICRE, V. FELL, D. STRAMSKI (2003b): Light scattering properties of marine particles in coastal and open ocean waters as related to the particle mass concentration. Limnol. Oceanogr., **48**, 843–859.

GORDON, H. R. (1993): Sensitivity of radiative transfer to small-angle scattering in the ocean: Quantitative assessment, Appl. Opt., **32**, 7505–7511.

GREGG, W. W. and K. L. CARDER (1990): A simple spectral solar irradiance model for cloudless maritime atmospheres, Limnol. Oceanogr., **35**, 1657–1675.

HARRISON, A. W. and C. A. COOMBES (1988): An opaque cloud cover model of sky short wavelength radiance, Solar Energy, **41**, 387–392.

HALTRIN, V. I. (2002): One-parameter two-term Henyey-Greenstein phase function for light scattering in seawater, Appl. Opt., **41**, 1022–1028.

MOBLEY, C. D. (1995): Hydrolight 3.0 User's Guide. SRI International, California.

MOBLEY, C. D., L. K. SUNDMAN and E. BOSS (2002): Phase function effects on oceanic light fields, Appl. Opt., **41**, 1035–1050.

MOORE, G. F., J. AIKEN and S. J. LAVENDER (1999): The atmospheric correction of water colour and the quantitative retrieval of suspended particulate matter in Case II waters, Int. J. Remote Sensing, **20**, 1713–1733.

MOREL, A. (1974): Optical properties of pure water and pure seawater, *In* Optical aspects of Oceanography, N.G.Jerlov and E.Steemann Nielsen (Eds.), Academic, New York, p.1–24.

MOREL, A. and S. MARITORENA (2001): Bio–optical properties of oceanic waters: A reappraisal, J. Geophys. Res., **106**, 7163–7180.

OISHI, T. (1990): Significant relationship between the backward scattering coefficient of sea water and the scatterance at 120°, Appl. Opt., **29**, 4658–4665.

PETZOLD, T. J. (1972): Volume scattering function for selected ocean waters SIO Ref.72–78, Scripps Inst. of Oceanogr., Univ. of California, San Diego.

PLASS, G. N., G. W. KATTAWAR and T. J. HUMPHREYS (1985): Influence of the oceanic scattering phase function on the radiance, J. Geophys. Res., **90**, C2, 3347–3351.

POPE, R. M and E. S. FRY (1997): Absorption spectrum (380–700nm) of pure water, Appl. Opt., **36**, 8710–8723.

Received March 8, 2007
Accepted August 9, 2007